

Ecodesign and 3D topology optimisation

Gustavo ASA*

DMSM, ISAE-SUPAERO, Toulouse, France

Supervised by: Joseph MORLIER

(Dated: August 27, 2023)

Abstract: This article aims to report the study on the use of topology optimisation methods for 3D printed eco-optimized structures. The first step consists in the validation of the extension of bidimensional optimisation of topology and fibre orientations so that it can be used in three dimensions. A complete optimisation was then performed considering both mechanical performance and environmental impact, showing the potential advantages that fibres of natural origin can provide to this kind of structures.

I. INTRODUCTION

The accelerated development of 3D printing technology has allowed the evolution of the existing methods for structural design, making viable the extensive use of topology optimisation, for example. Composite materials are also becoming of great importance in the aerospace industry, and materials of natural origin are as well subject of this study, with the goal of building efficient eco-optimised structures.

For isotropic optimisations, the material choice can be decoupled from the topology optimisation [1]. However, the mechanical properties of anisotropic materials influence the final geometry obtained, so that the optimisation has to be done simultaneously to the material choice.

The objective of this work is to study the use of topology optimisation algorithms to design 3D printable structures while taking into account their environmental impact along with their mechanical performance.

The remainder of this article is organised as follows. In section II a brief approach is made to some concepts necessary to the development of the work carried out. In section III is a description of the work done throughout the project. Then some results are presented and discussed in section IV. Conclusions are drawn in section ?? and some future work in the scope of this project is proposed in section ??.

II. LITERATURE REVIEW

A. Solid Isotropic Material with Penalization (SIMP)

Solid Isotropic Material with Penalisation (SIMP) is a finite element-based method for topology optimisation. For each element, a density value ρ_e within the range from 0 (void element) to 1 (filled element) is assigned. To enforce the convergence to a predominantly 0/1 configuration (the only physically feasible values, there is no intermediate material), the material properties for each element are obtained from a power-law interpolation, i.e. dependent on ρ_e^p , where p is a penalisation factor (typically $p = 3$).

Sigmund [2] defines then a topology optimisation problem where the objective is to minimise compliance:

$$\begin{aligned} \min_{\rho} c(\rho) &= \mathbf{U}^T \mathbf{K} \mathbf{U} = \sum_e \rho_e^p \mathbf{u}_e^T \mathbf{k}_0 \mathbf{u}_e^T \\ \text{subject to } &\begin{cases} \frac{V(\rho)}{V_0} \leq f \\ \mathbf{K} \mathbf{U} = \mathbf{F} \\ 0 < \rho_{min} \leq \rho \leq 1 \end{cases} \end{aligned} \quad (1)$$

where \mathbf{U} and \mathbf{F} are the global displacement and force vectors, respectively, \mathbf{K} is the global stiffness matrix, \mathbf{u}_e and $\mathbf{k}_e = \rho_e^p \mathbf{k}_0$ are the element displacement vector and stiffness matrix, respectively, ρ is the vector of design variables, ρ_{min} is the minimum relative density (non-zero to avoid singularity), $V(\rho)$ and V_0 are the material volume and design domain volume, and f is the prescribed volume fraction.

The optimisation problem can be solved using various methods such as Optimality Criteria (OC) [3], Sequential Linear Programming (SLP) [4], the Method of Moving Asymptotes (MMA) [5], and others.

To avoid the appearance of checkerboard patterns and to ensure the mesh-independence of the result, the element sensitivities are filtered by a linear decaying convolution filter:

$$\rho_e \widetilde{\frac{\partial c}{\partial \rho_e}} = \frac{\sum_i H_{ei}^\rho \rho_i \frac{\partial c}{\partial \rho_i}}{\sum_i H_{ei}^\rho} \quad (2)$$

$$H_{ei}^\rho = \max(0, r_\rho - \Delta(e, i)) \quad (3)$$

where r_ρ is a fixed filter radius and the $\Delta(e, i)$ operator is the distance between the centers of elements e and i .

B. Continuous Fiber Angle Optimisation (CFAO)

For a given domain, the determination of fibre orientations can be performed using various approaches. A method that emerged is the Discrete Material Optimisation (DMO), in which the orientations are chosen from a predefined finite set of possibilities, defining different materials that can be used. It is useful for composite

laminates for example, but it is not suitable for 3D printing as it does not ensure fibre continuity. On the other side of the spectrum, Free Material Optimisation (FMO) treats the stiffness tensor components as design variables, increasing the freedom in the design, although sometimes leading to infeasible material properties.

In Continuous Fibre Angle Optimisation (CFAO), an orientation is assigned for each finite element, a methodology that can be easily integrated to the SIMP method and adjusted to yield continuous orientations over the domain. However, this approach may present local minima due to the periodicity of the angle, that can be avoided by using the correct representation of the orientations with the design variables.

C. SIMP extended with CFAO

The SIMP method can then be extended with CFAO creating a modified 2D problem where both sets of variables are simultaneously optimised [6]:

$$\begin{aligned} \min_{\rho, \theta} c(\rho, \theta) &= \sum_e \rho_e^p \mathbf{u}_e^T \mathbf{k}_0(\theta_e) S \mathbf{u}_e^T \\ \text{subject to } &\left\{ \begin{array}{l} \frac{V(\rho)}{V_0} \leq f \\ \mathbf{KU} = \mathbf{F} \\ 0 < \rho_{min} \leq \rho \leq 1 \\ -2\pi \leq \theta \leq 2\pi \end{array} \right. \end{aligned} \quad (4)$$

As some problems may arise from the periodicity of the angle variable, another possible approach is to define the orientation using the Cartesian components of the orientation vector [7].

In all formulations, a filter is necessary to regularise the orientations and create a smoothly varying field that can be more easily converted to a printable structure. There is a wider range of choices for this filter, which is independent of the filter applied to the densities. Within each iteration, it can be applied on the sensitivities [8], on the material tensor [9], on the angles [10], or on the angles Cartesian projections [11]. Furthermore, the type of filter can also vary, such as using a Gaussian filter instead of the convolution filter with weights decaying linearly [8].

Finally, there are multiple possibilities to extend the problem to 3D, with varying levels of computational cost, manufacturing easiness, and design space freedom:

- Choose a printing direction and divide the domain in layers [6]
- Define allowable printing planes to make components that can be later assembled [11]
- Optimise geometric primitives (plates, bars) as discrete components [12, 13]

- Introduce design variables to define free 3D fibre orientations by spherical coordinates azimuth and elevation [10]

D. Design for 3D printing

intro to additive manufacturing

The hatch spacing and the printing radius are the main additional properties which are constrained due to the manufacturing process. The minimum printing radius can be controlled by the filter applied to the orientations during the optimisation, but both constraints can be added to the final design during the printing path planning [14].

When printing geometries that were optimised as 2D, the out-of-plane direction can be used as printing direction without further modifications. On the other hand, when all three dimensions are free to be optimised, supports may be required, which increase the printing time and the material consummation. If one judges that it is necessary to avoid them, an overhang constraint can be added to the optimisation to make self-supporting structures with a low cost in compliance, but introducing computational difficulties due to nonlinearities [15]. If not, supports can be added when preparing the piece to be printed.

After the optimisation, an important step is to convert the result in a printable piece. Papapetrou, Patel, and Tamijani [16] compare different infill methods, which convert the optimised orientations into continuous fibre paths. The two more robust methods presented are the streamline method, which determines streamlines based on the optimised orientation vector field, and the offset method, in which the fibres are obtained parallel to the optimised lay-out. Also, the optimisation algorithm benefits from introducing these methods in the last iterations.

Another option is presented by Huang et al. [14], where the structure is divided in finite sections forming a graph. Inside each section, the fiber trajectory is given by the optimised orientations, while the global trajectory is a Hamilton path in the graph. Hence, the whole structure can be converted in a single continuous path and with no fibre breaks.

III. DEVELOPED WORK

A. Implementation

The algorithm was implemented in Python, using the Method of Moving Asymptotes (MMA) [5] as variable updating scheme and Ansys as external finite element solver. The latter allows a straightforward creation of the mesh and boundary conditions, which might be time-consuming to perform by hand for complex 3D geometries.

The global stiffness matrix assemblage step is then abstracted, but the algorithm is still dependent on the construction of elemental stiffness matrices \mathbf{k}_0 to calculate sensitivities. Therefore, the implementation constraints which element types can be used in the Ansys model.

For 2D optimisations, the implementation assumes a 4-node quadrilateral element (Ansys element type PLANE182), whose form functions N_i and strain-displacement matrix \mathbf{B}_e are

$$\begin{Bmatrix} N_1 \\ N_2 \\ N_3 \\ N_4 \end{Bmatrix} (r, s) = \frac{1}{4} \begin{Bmatrix} (1-r)(1-s) \\ (1+r)(1-s) \\ (1+r)(1+s) \\ (1-r)(1+s) \end{Bmatrix} \quad (5)$$

$$\mathbf{B}_e = \begin{bmatrix} \frac{\partial N_1}{\partial r} & 0 & \dots & \frac{\partial N_4}{\partial r} & 0 \\ 0 & \frac{\partial N_1}{\partial s} & \dots & 0 & \frac{\partial N_4}{\partial s} \\ \frac{\partial N_1}{\partial s} & \frac{\partial N_1}{\partial r} & \dots & \frac{\partial N_4}{\partial s} & \frac{\partial N_4}{\partial r} \end{bmatrix} \quad (6)$$

For 3D optimisations, the implementation assumes an 8-node brick element (SOLID185):

$$\begin{Bmatrix} N_1 \\ N_2 \\ N_3 \\ N_4 \\ N_5 \\ N_6 \\ N_7 \\ N_8 \end{Bmatrix} (r, s, t) = \frac{1}{8} \begin{Bmatrix} (1-r)(1-s)(1-t) \\ (1+r)(1-s)(1-t) \\ (1+r)(1+s)(1-t) \\ (1-r)(1+s)(1-t) \\ (1-r)(1-s)(1+t) \\ (1+r)(1-s)(1+t) \\ (1+r)(1+s)(1+t) \\ (1-r)(1+s)(1+t) \end{Bmatrix} \quad (7)$$

$$\mathbf{B}_e = \begin{bmatrix} \frac{\partial N_1}{\partial r} & 0 & 0 & \dots & \frac{\partial N_8}{\partial r} & 0 & 0 \\ 0 & \frac{\partial N_1}{\partial s} & 0 & \dots & 0 & \frac{\partial N_8}{\partial s} & 0 \\ 0 & 0 & \frac{\partial N_1}{\partial t} & \dots & 0 & 0 & \frac{\partial N_8}{\partial t} \\ 0 & \frac{\partial N_1}{\partial t} & \frac{\partial N_1}{\partial r} & \dots & 0 & \frac{\partial N_8}{\partial t} & \frac{\partial N_8}{\partial r} \\ \frac{\partial N_1}{\partial t} & 0 & \frac{\partial N_1}{\partial s} & \dots & \frac{\partial N_8}{\partial t} & 0 & \frac{\partial N_8}{\partial s} \\ \frac{\partial N_1}{\partial s} & \frac{\partial N_1}{\partial r} & 0 & \dots & \frac{\partial N_8}{\partial s} & \frac{\partial N_8}{\partial r} & 0 \end{bmatrix} \quad (8)$$

B. Problem formulation

Similarly to Schmidt et al. [10], the fibre orientations were defined using two spherical coordinates: θ_e (rotation in the xy plane, positive from x towards y) and α_e (rotation in the new yz plane, positive from y towards z). The design variables are then ρ , θ , and α , so that the optimisation problem is written as

$$\begin{aligned} \min_{\rho, \theta, \alpha} c(\rho, \theta, \alpha) &= \sum_e \rho_e^p \mathbf{u}_e^T \mathbf{k}_0(\theta_e, \alpha_e) \mathbf{u}_e^T \\ \text{s.t. } &\left\{ \begin{array}{l} \frac{V(\rho)}{V_0} \leq f \\ \mathbf{KU} = \mathbf{F} \\ 0 < \rho_{min} \leq \rho \leq 1 \\ -\pi \leq \theta \leq \pi \\ -2\pi \leq \alpha \leq 2\pi \end{array} \right. \end{aligned} \quad (9)$$

The algorithm can be adapted to restrict orientations to the xy plane by removing the α variables. By also removing the θ variables, the SIMP method is recovered. Lastly, the assumption of 2D or 3D optimisation lies on the definition of \mathbf{k}_0 .

Densities were filtered using the convolution filter in Eq. 2. For orientation smoothing, a similar convolution filter was applied directly to the angles at each iteration, adjusted to reduce the weight of void elements on the average:

$$\begin{Bmatrix} \tilde{\theta}_e \\ \tilde{\alpha}_e \end{Bmatrix} = \frac{1}{\sum_i H_{ei}^\theta \rho_i} \sum_i H_{ei}^\theta \rho_i \begin{Bmatrix} \theta_i \\ \alpha_i \end{Bmatrix} \quad (10)$$

$$H_{ei}^\theta = \max(0, r_\theta - \Delta(e, i)) \quad (11)$$

where r_θ is independent from r_ρ and is related to the desired minimum fiber curvature

C. Material modeling

The materials were modeled as transverse isotropic, suitable for matrices reinforced by unidirectional fibres. The fibres were considered to be aligned with the local x axis, which can be characterised by five independent elastic constants: longitudinal Young modulus E_x , transversal Young modulus E_y , in-plane Poisson's ratio ν_{xy} , out-of-plane Poisson's ratio ν_{yz} , and in-plane shear modulus G_{xy} .

The rule of mixtures was used to estimate the elastic constants of the composite material. For a fibre volume fraction of V_f , the material in-plane constants are written as [17]

$$E_x = E_f V_f + E_m (1 - V_f) \quad (12)$$

$$E_y = \frac{E_f E_m}{E_f (1 - V_f) + E_m V_f} \quad (13)$$

$$\nu_{xy} = \nu_f V_f + \nu_m (1 - V_f) \quad (14)$$

$$G_{xy} = \frac{G_f G_m}{G_f (1 - V_f) + G_m V_f} \quad (15)$$

where E_f , ν_f , G_f are the fibre properties and E_m , ν_m , G_m are the matrix properties. Finally, ν_{yz} is defined by symmetries in 3D elasticity [18]

$$\nu_{yz} = \nu_{xy} \frac{1 - \nu_{xy} \frac{E_y}{E_x}}{1 - \nu_{xy}} \quad (16)$$

The constitutive matrix \mathbf{C} for transverse isotropic materials is given by

$$\mathbf{C} = \begin{bmatrix} \frac{1}{E_x} & -\frac{\nu_{xy}}{E_x} & -\frac{\nu_{xy}}{E_x} & 0 & 0 & 0 \\ -\frac{\nu_{xy}}{E_x} & \frac{1}{E_y} & -\frac{\nu_{yz}}{E_y} & 0 & 0 & 0 \\ -\frac{\nu_{xy}}{E_x} & -\frac{\nu_{yz}}{E_y} & \frac{1}{E_y} & 0 & 0 & 0 \\ 0 & 0 & 0 & \frac{2(1+\nu_{yz})}{E_y} & 0 & 0 \\ 0 & 0 & 0 & 0 & \frac{1}{G_{xy}} & 0 \\ 0 & 0 & 0 & 0 & 0 & \frac{1}{G_{xy}} \end{bmatrix}^{-1} \quad (17)$$

The final material orientation within an element is obtained by a rotation θ around the z axis followed by a rotation α around the x axis, after which the rotated constitutive matrix \mathbf{C}_r is written as

$$\mathbf{C}_r(\theta_e, \alpha_e) = \mathbf{T}_\alpha(\alpha_e) \mathbf{T}_\theta(\theta_e) \mathbf{C} \mathbf{T}_\theta^T(\theta_e) \mathbf{T}_\alpha^T(\alpha_e) \quad (18)$$

$$\mathbf{T}_\theta(\theta_e) = \begin{bmatrix} c_\theta^2 & s_\theta^2 & 0 & 0 & 0 & -2s_\theta c_\theta \\ s_\theta^2 & c_\theta^2 & 0 & 0 & 0 & 2s_\theta c_\theta \\ 0 & 0 & 1 & 0 & 0 & 0 \\ 0 & 0 & 0 & c_\theta & s_\theta & 0 \\ 0 & 0 & 0 & -s_\theta & c_\theta & 0 \\ c_\theta s_\theta & -c_\theta s_\theta & 0 & 0 & 0 & c_\theta^2 - s_\theta^2 \end{bmatrix} \quad (19)$$

$$\mathbf{T}_\alpha(\alpha_e) = \begin{bmatrix} 1 & 0 & 0 & 0 & 0 & 0 \\ 0 & c_\alpha^2 & s_\alpha^2 & -2c_\alpha s_\alpha & 0 & 0 \\ 0 & s_\alpha^2 & c_\alpha^2 & 2c_\alpha s_\alpha & 0 & 0 \\ 0 & c_\alpha s_\alpha & -c_\alpha s_\alpha & c_\alpha^2 - s_\alpha^2 & 0 & 0 \\ 0 & 0 & 0 & 0 & c_\alpha & s_\alpha \\ 0 & 0 & 0 & 0 & -s_\alpha & c_\alpha \end{bmatrix} \quad (20)$$

where $c_\theta = \cos \theta_e$, $s_\theta = \sin \theta_e$, $c_\alpha = \cos \alpha_e$, $s_\alpha = \sin \alpha_e$.

D. Sensitivity analysis

As the MMA is gradient-based, it is necessary to calculate the sensitivities of the objective function with respect to the design variables. Its expression

$$c(\rho, \theta, \alpha) = \sum_e \rho_e^p \mathbf{u}_e^T \mathbf{k}_0(\theta_e, \alpha_e) \mathbf{u}_e^T \quad (21)$$

leads to

$$\frac{\partial c}{\partial \rho_e} = -p \rho_e^{p-1} \mathbf{u}_e^T \mathbf{k}_0 \mathbf{u}_e^T \quad (22)$$

$$\frac{\partial c}{\partial \theta_e} = -\rho_e^p \mathbf{u}_e^T \frac{\partial \mathbf{k}_0}{\partial \theta_e} \mathbf{u}_e^T \quad (23)$$

$$\frac{\partial c}{\partial \alpha_e} = -\rho_e^p \mathbf{u}_e^T \frac{\partial \mathbf{k}_0}{\partial \alpha_e} \mathbf{u}_e^T \quad (24)$$

The value of \mathbf{k}_0 is not explicitly calculated during the optimisation, as each value of $\rho_e^p \mathbf{u}_e^T \mathbf{k}_0(\theta_e, \alpha_e) \mathbf{u}_e^T$ corresponds to the elemental strain energy and can be gathered from Ansys. On the other hand, the derivatives $\frac{\partial \mathbf{k}_0}{\partial \theta_e}$

and $\frac{\partial \mathbf{k}_0}{\partial \alpha_e}$ need to be integrated since these matrices are not directly accessible as Ansys results:

$$\begin{aligned} \frac{\partial \mathbf{k}_0}{\partial \theta_e}(\theta_e, \alpha_e) = & \int \int \int \mathbf{B}_e^T \mathbf{T}_\alpha \left(\frac{\partial \mathbf{T}_\theta}{\partial \theta_e} \mathbf{C} \mathbf{T}_\theta^T + \mathbf{T}_\theta \mathbf{C} \frac{\partial \mathbf{T}_\theta^T}{\partial \theta_e} \right) \mathbf{T}_\alpha^T \mathbf{B}_e d\Omega \end{aligned} \quad (25)$$

$$\begin{aligned} \frac{\partial \mathbf{k}_0}{\partial \alpha_e}(\theta_e, \alpha_e) = & \int \int \int \mathbf{B}_e^T \left(\frac{\partial \mathbf{T}_\alpha}{\partial \alpha_e} \mathbf{T}_\theta \mathbf{C} \mathbf{T}_\theta^T \mathbf{T}_\alpha^T + \mathbf{T}_\alpha \mathbf{T}_\theta \mathbf{C} \mathbf{T}_\theta^T \frac{\partial \mathbf{T}_\alpha^T}{\partial \alpha_e} \right) \mathbf{B}_e d\Omega \end{aligned} \quad (26)$$

Proper simplifications were applied for the 2D and 3D with in-plane orientations cases. Each integral was numerically evaluated with 2-point Gaussian quadrature, which is exact since the expressions are linear in each natural coordinate for the chosen element formulations.

E. CO₂ footprint assessment

In this work, the environmental impact of the structure is measured in terms of the mass of CO₂ emitted during material production and during its use in a long distance aircraft, following the methodology from Duriez et al. [1], adapted to composite materials.

Firstly, the material density ρ was calculated from the fibre and matrix densities ρ_f and ρ_m :

$$\rho = \rho_f V_f + \rho_m (1 - V_f) \quad (27)$$

The impact of the material production $CO_{2,mat}$ depends on the total mass M and the CO₂ intensity of the material $CO_{2,mat}^i$ (mass of CO₂ emitted per mass of material):

$$CO_{2,mat} = M \cdot CO_{2,mat}^i, \quad (28)$$

where $CO_{2,mat}^i$ depends on the CO₂ intensities of the fibre and matrix, $CO_{2,f}^i$ and $CO_{2,m}^i$:

$$CO_{2,mat}^i = \frac{\rho_f V_f CO_{2,f}^i + \rho_m (1 - V_f) CO_{2,m}^i}{\rho} \quad (29)$$

The impact of the use phase $CO_{2,use}$ is calculated as the amount of emissions that would be saved if the component was lighter. Reducing the mass by 1 kg in a long distance aircraft leads to a reduction of 98.8 tCO₂ during its lifetime [1], therefore

$$CO_{2,use} = M \cdot 98.8 \text{ tCO}_2/\text{kg} \quad (30)$$

The value used to compare different designs is the total footprint $CO_{2,tot}$:

$$CO_{2,tot} = CO_{2,mat} + CO_{2,use} \quad (31)$$

IV. RESULTS

A. Bridge

The first numerical experiment aims to make a comparison with results obtained by Greifenstein et al. [13], who made a 2D optimisation based on curved splines (“anisotropic spaghetti”). The problem consists in optimise the bridge shown in Fig. 1 subject to a 0.5 MPa pressure on top. The bridge has dimensions 2 m × 1 m and a layer of solid elements is prescribed near the top edge.

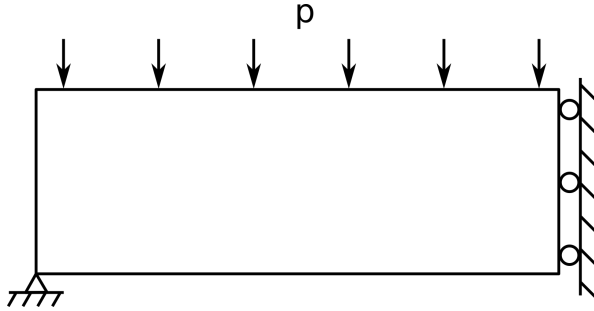


Figure 1: Bridge problem.

The material used is a carbon fiber reinforced polymer (CFRP) with mechanical properties given in Table I.

Table I: Carbon-epoxy mechanical properties.

E_x (GPa)	E_y (GPa)	ν_{xy}	G_{xy} (GPa)
113.6	9.650	0.334	6.0

The anisotropic spaghetti optimisation result is shown in Fig. 2 and has a compliance of 0.225 N.m.

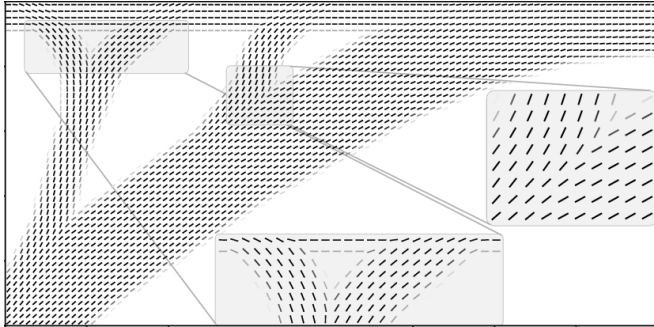


Figure 2: Bridge optimised with anisotropic spaghetti [13].

For the Extended SIMP method, the domain was divided in a 100×50 mesh, summing up to 5000 square elements and 10000 design variables. Optimisation parameters were set at $f = 0.4$, $r_\rho = 70$ mm, and $r_\theta = 160$ mm.

As the result is strongly sensitive to the initial fiber orientation, the optimisation was performed using 19 different initial angles between -90° and 90° . Additionally, an optimisation with randomly chosen orientations for each element was performed, which should be a good approximation for the global minimum when the optimal initial orientation is not known [10].

Figure 3 shows the final compliance of each run after 100 iterations and the strong influence of the initial conditions on finding local minima. In terms of compliance, the best design found, shown in Fig. 4, starts from an initial angle of 70° , with a final compliance of 0.218 N.m. Another result important to point out is the one with initial angle of 40° , shown in Fig. 5, which is also near optimal with a compliance of 0.220 N.m and its overall form is closer to 2. [convergence plot with images](#)

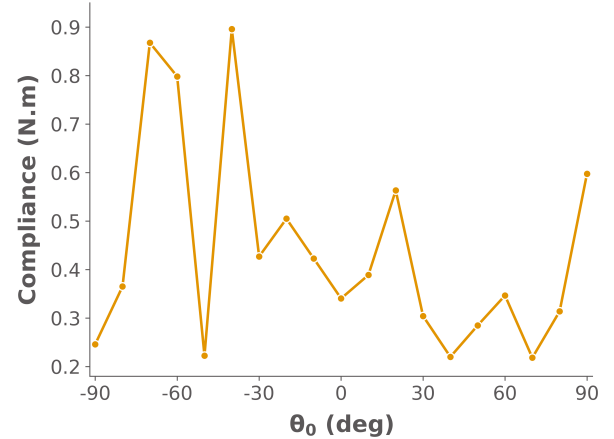


Figure 3: Dependence of final compliance on initial orientation.

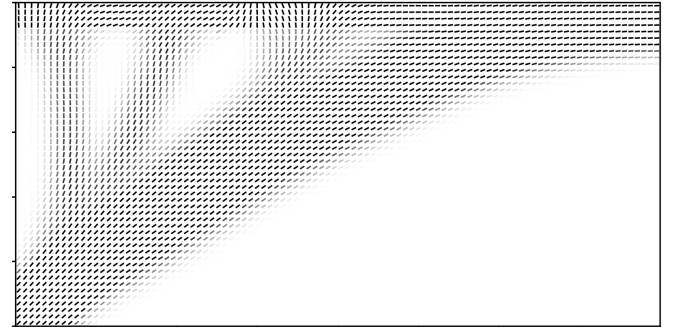


Figure 4: Final bridge design with initial orientation of 70° . [add zoom](#)

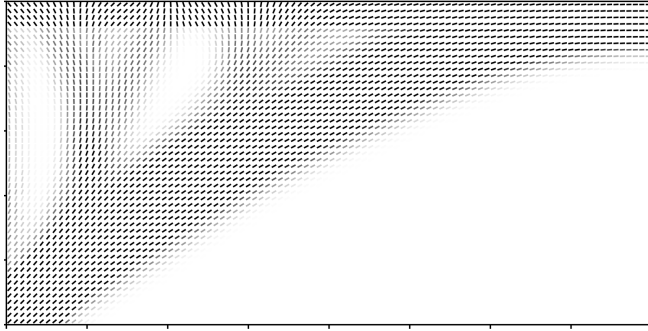


Figure 5: Final bridge design with initial orientation of 40°. [add zoom](#)

The designs do not match exactly, which is expected since the methods are based on different design parameters that cannot be completely translated. Nonetheless, the final geometries are qualitatively similar and the numerical values differ by only 3%.

Due to the use of discrete components and an initial condition similar to the result in Fig. 5, the spaghetti design could not converge to a design similar to Fig. 4, with a slightly lower compliance. On the other hand, the spaghetti formulation has a good handling of material-void transition, while the density-based solutions show some grayness instead of the smaller void areas. To address this problem, it would be necessary to add projections of the density variables to force a result closer to binary, such as in Nomura et al. [7].

Running the optimisation with various initial conditions is an expensive approach, especially if it is inside an outer loop varying other parameters. Figure 6 shows the result of an optimisation with random initial orientations, presenting a compliance of 0.230 N.m. It is not as regular as the previous designs, but it is relatively similar to the optimal point, both qualitatively and quantitatively. This approach can then be used as a computationally cheaper approximation to the true optimum, although it may require some post processing.

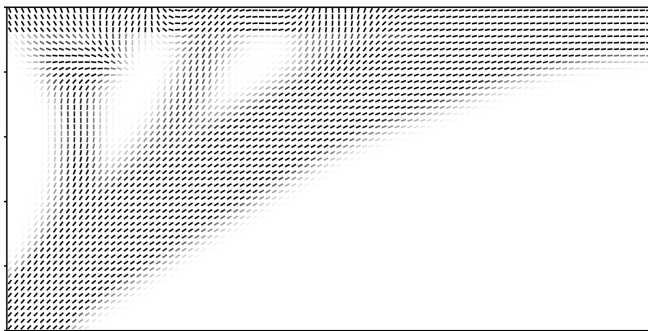


Figure 6: Final bridge design with random initial orientations. [add zoom](#)

B. MBB Beam

The second numerical experiment aims to validate the extension of the problem formulation from two to three dimensions, by verifying the equivalence between the optimisations of an extruded geometry using 2D and 3D elements.

The reference problem is a half Messerschmitt–Bölkow–Blohm (MBB) beam, with boundary conditions shown in Fig. 7. The optimisation was performed in a 186 mm × 80 mm × 8 mm half beam, under a 1 kN force.

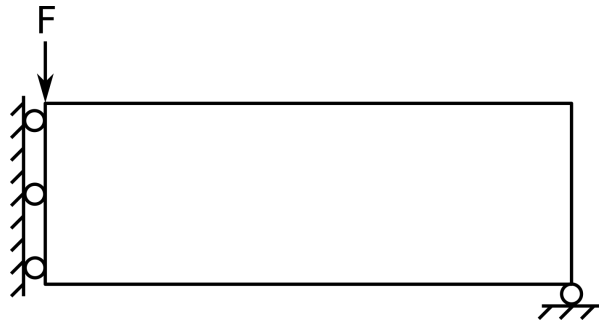


Figure 7: Half MBB beam problem.

The domain was divided in 2D and 3D elements with side length equal to 4 mm. For both meshes, the problem was solved for $f = 0.3$, $r_\rho = 8$ mm, $r_\theta = 20$ mm, and initial orientation of 50°. As the filter radii are greater than the domain thickness, all layers (in z direction) of the 3D design are forced to be nearly equal, which should result in a final geometry equivalent to the 2D case. Table II presents the mechanical properties considered, corresponding to a cellulose matrix reinforced with 0.5 volume fraction of bamboo fibre.

Table II: Bamboo-cellulose mechanical properties.

E_x (GPa)	E_y (GPa)	ν_{xy}	G_{xy} (GPa)
10.37	5.48	0.1975	2.1

Figure 8 shows the compliance history over 150 iterations. The 2D optimisation reached a compliance of 2691 N.mm, while the 3D reached 2733 N.mm, which corresponds to a relative difference of 1.6%. Fig. 9 and 10 show the final geometries obtained, which are almost identical, indicating the good correspondence between both problem formulations.

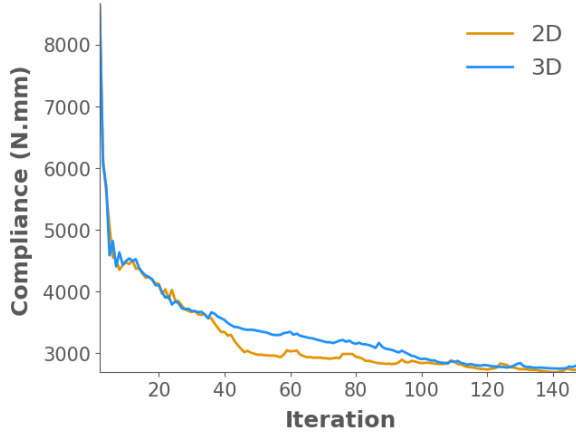


Figure 8: Compliance history for MBB beam optimisation.

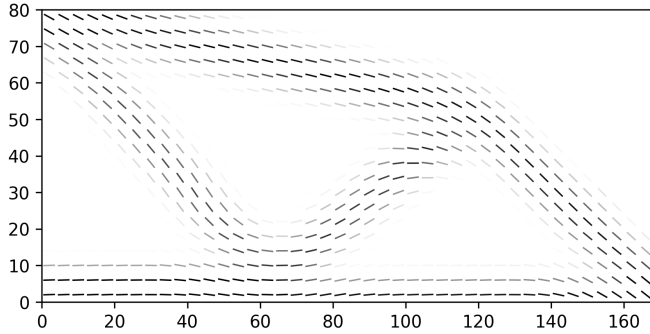


Figure 9: 2D optimisation final design. Compliance = 2691 N.mm.

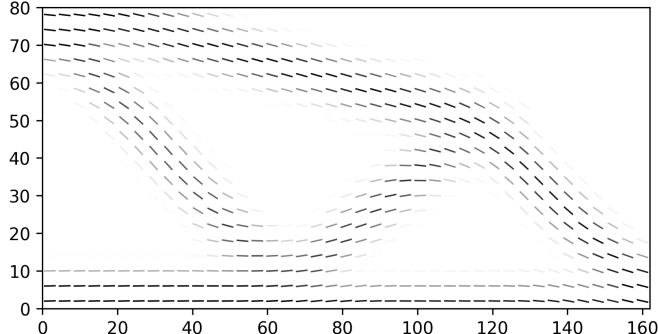


Figure 10: Bottom layer of the 3D optimisation final design. Compliance = 2733 N.mm.

In this configuration, the 3D optimisation provides more freedom on the spatial material distribution, allowing more efficient structures. The drawbacks are a slightly slower convergence, as depicted in Fig. 8, and a higher computation time due to the increased number of design variables and degrees of freedom in the finite element model.

C. MBB beam material optimisation

A material optimisation was performed on the same MBB beam, using 3D elements with side length equal to 2 mm. For all run cases, orientations were defined by in-plane rotations, the filter parameters were set as $r_\rho = 4$ mm and $r_\theta = 10$ mm, and initial angles were randomly chosen for each element.

All possible combinations of fibres in Table III and resins in Table IV were tested, with fibre volume fractions of 0.25 and 0.5. Each material combination was optimised for f varying from 0.2 to 0.55 for 80 iterations of the MMA algorithm.

Table III: Material properties of available fibres.

Fibre	ρ_f (kg/m ³)	E_f (GPa)	ν_f	$CO_{2,f}^i$ (kg CO ₂ /kg)
Bamboo	700	17.5	0.04	1.0565
Flax	1470	53.5	0.355	0.44
Hemp	1490	62.5	0.275	1.6
Carbon High Modulus	2105	760	0.105	68.1
Carbon Low Modulus	1820	242.5	0.105	20.3
S-Glass	2495	89.5	0.22	2.905
E-Glass	2575	78.5	0.22	2.45

Table IV: Material properties of available resins.

Resin	ρ_m (kg/m ³)	E_m (GPa)	ν_m	$CO_{2,m}^i$ (kg CO ₂ /kg)
Cellulose	990	3.25	0.355	3.8
PLA	1290	5.19	0.39	2.115
PETG (abs)	1270	2.06	0.403	4.375
Epoxy	1255	2.41	0.399	5.94
Polyester	1385	4.55	0.35	4.5

Figure 11 shows compliance and CO₂ footprint for the designs obtained with $f = 0.3$. It can be seen that natural fibres are more efficient as their points are positioned closer to the origin. For a fixed value of f , if the goal is to minimise $CO_{2,tot}$, bamboo appears as the best choice of fibre. Furthermore, to obtain stiffer structures with a good compromise with $CO_{2,tot}$, flax and hemp are better options than carbon and glass fibres.

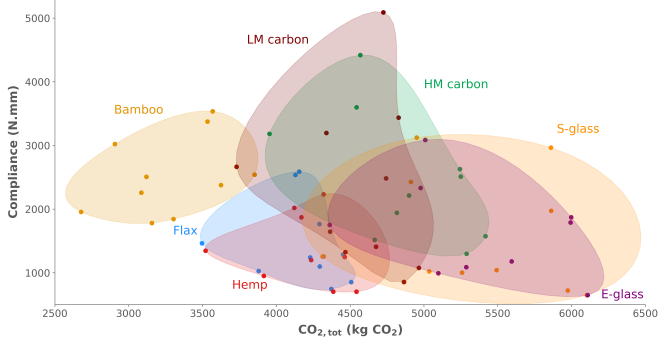


Figure 11: Compliance and CO₂ footprint for $f = 0.3$, all materials.

Regarding the resins, Fig. 12 shows that cellulose is the most efficient resin to be used as matrix reinforced by the natural fibres, but PLA and polyester are also viable options.

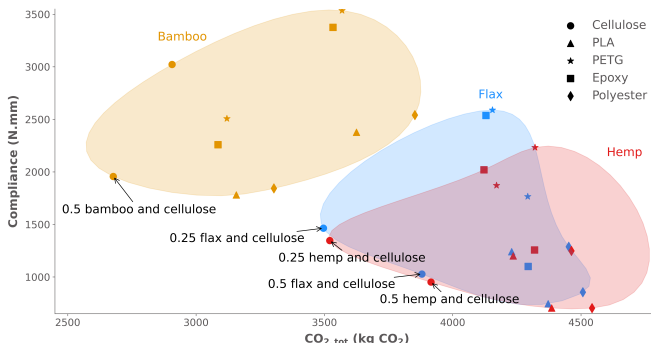


Figure 12: Compliance and CO₂ footprint for $f = 0.3$, natural fibres.

The volume fraction constraint f also plays an important role in obtaining the most efficient structure. Figure 13 shows the results obtained for each value of f . Most of the designs in the Pareto front are made of flax or hemp, indicating that they can be more efficient than bamboo structures by achieving the same compliance with lower volume fraction, which generally implies lower mass and lower carbon footprint. Bamboo structures are the most efficient only for the lowest volume fractions, where the width of the solid regions reaches the minimum allowed by the filter and cannot be further reduced. The main goal of these structures is to reduce carbon footprint at the cost of higher compliance. On the other side of the spectrum, the structures with $f = 0.55$ do not appear on the Pareto front, showing that material is allocated on non-essential regions, leading to a higher mass without a substantial gain in compliance. While it is not possible to increase the volume fraction, fibreglass becomes the most efficient fibre if the goal is to minimise compliance. It is then clear that the characteristics of the optimal design change with respect to the desired compromise between compliance and carbon footprint.

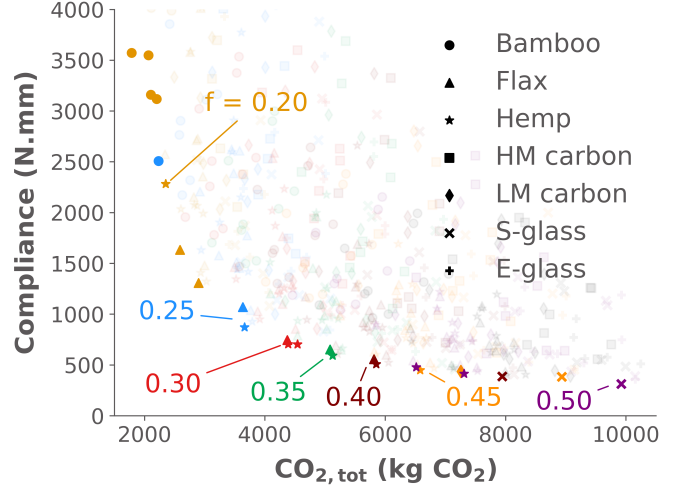
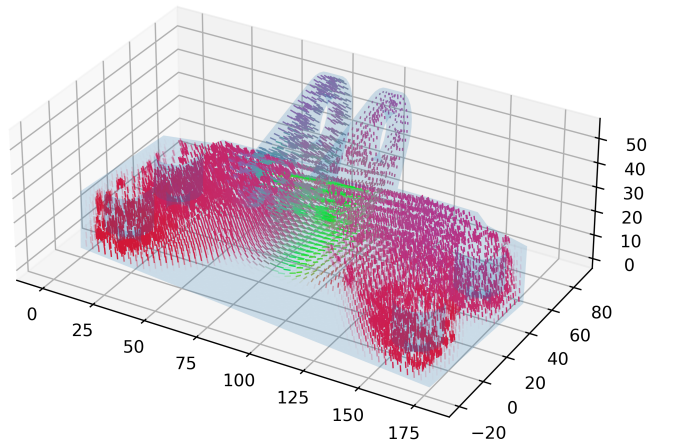


Figure 13: Pareto front of all optimised material-volume configurations.

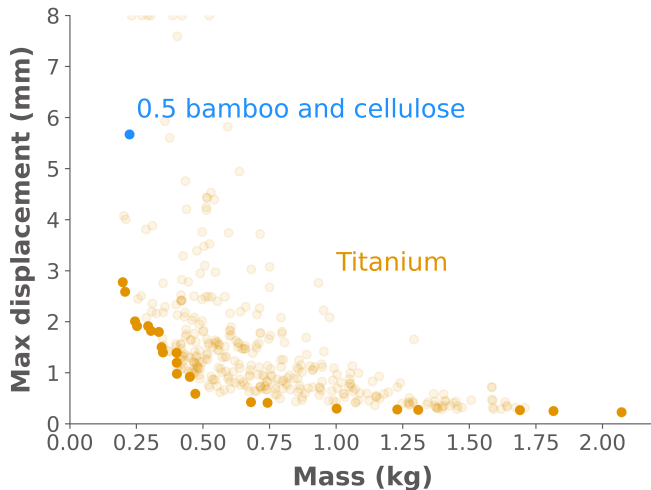
Finally, as the optimisations were performed with random initial orientations, the points obtained should be close to but may not correspond to the respective global minima. Therefore, after choosing the appropriate material and volume fraction combination, the optimisation process can be run again for this specific configuration with various initial conditions to find designs more efficient than the one already obtained.

D. Bracket

bracket [19]



results [20]



V. CONCLUSION

conclusion

VI. FUTURE WORK

future work

VII. ACKNOWLEDGEMENTS

acknowledgements

REFERENCES

- [1] Edouard Duriez et al. “Ecodesign with topology optimization”. In: *Procedia CIRP* 109 (2022), pp. 454–459.
- [2] Ole Sigmund. “A 99 line topology optimization code written in Matlab”. In: *Structural and multidisciplinary optimization* 21 (2001), pp. 120–127.
- [3] Martin Philip Bendsoe and Ole Sigmund. *Topology optimization: theory, methods, and applications*. Springer Science & Business Media, 2003.
- [4] Pauli Pedersen. *The integrated approach of FEM-SLP for solving problems of optimal design*. Technical University of Denmark, 1980.
- [5] Krister Svanberg. “The method of moving asymptotes—a new method for structural optimization”. In: *International journal for numerical methods in engineering* 24.2 (1987), pp. 359–373.
- [6] Delin Jiang, Robert Hoglund, and Douglas E Smith. “Continuous fiber angle topology optimization for polymer composite deposition additive manufacturing applications”. In: *Fibers* 7.2 (2019), p. 14.
- [7] Tsuyoshi Nomura et al. “General topology optimization method with continuous and discrete orientation design using isoparametric projection”. In: *International Journal for Numerical Methods in Engineering* 101.8 (2015), pp. 571–605.
- [8] Enrico Stragiotti. “Continuous Fiber Path Planning Algorithm for 3D Printed Optimal Mechanical Properties.” MA thesis. Politecnico di Torino, 2020.
- [9] Dustin R Jantos, Klaus Hackl, and Philipp Junker. “Topology optimization with anisotropic materials, including a filter to smooth fiber pathways”. In: *Structural and Multidisciplinary Optimization* 61 (2020), pp. 2135–2154.
- [10] Martin-Pierre Schmidt et al. “Structural topology optimization with smoothly varying fiber orientations”. In: *Structural and Multidisciplinary Optimization* 62 (2020), pp. 3105–3126.
- [11] Zheng Qiu et al. “Concurrent topology and fiber orientation optimization method for fiber-reinforced composites based on composite additive manufacturing”. In: *Computer Methods in Applied Mechanics and Engineering* 395 (2022), p. 114962.
- [12] Hollis Smith and Julián A Norato. “Topology optimization with discrete geometric components made of composite materials”. In: *Computer Methods in Applied Mechanics and Engineering* 376 (2021), p. 113582.
- [13] Jannis Greifenstein et al. “Efficient spline design via feature-mapping for continuous fiber-reinforced structures”. In: *Structural and Multidisciplinary Optimization* 66.5 (2023), p. 99.
- [14] Yiming Huang et al. “Multiscale concurrent design and 3D printing of continuous fiber reinforced thermoplastic composites with optimized fiber trajectory and topological structure”. In: *Composite Structures* 285 (2022), p. 115241.
- [15] Andrew T Gaynor and James K Guest. “Topology optimization considering overhang constraints: Eliminating sacrificial support material in additive manufacturing through design”. In: *Structural and Multidisciplinary Optimization* 54.5 (2016), pp. 1157–1172.
- [16] Vasileios S Papapetrou, Chitrang Patel, and Ali Y Tami-jani. “Stiffness-based optimization framework for the topology and fiber paths of continuous fiber composites”. In: *Composites Part B: Engineering* 183 (2020), p. 107681.
- [17] Robert M Jones. *Mechanics of composite materials*. 1st ed. New York: McGraw-Hill, 1975.
- [18] Richard M Christensen. “Tensor transformations and failure criteria for the analysis of fiber composite materials”. In: *Journal of Composite Materials* 22.9 (1988), pp. 874–897.
- [19] GrabCAD. *GrabCAD GE jet engine bracket challenge*. [Accessed: 07 July 2023]. 2013. URL: <https://grabcad.com/challenges/ge-jet-engine-bracket-challenge>.
- [20] Eamon Whalen, Azariah Beyene, and Caitlin Mueller. “SimJEB: Simulated Jet Engine Bracket Dataset”. In: *Computer Graphics Forum* (2021).